PERGAMON

International Journal of Solids and Structures 39 (2002) 367–392

INTERNATIONAL JOURNAL OF SOLIDS and STRUCTURES

www.elsevier.com/locate/ijsolstr

Buckle propagation in pipe-in-pipe systems. Part II. Analysis

Stelios Kyriakides *, Tracy J. Vogler

Research Center for Mechanics of Solids, Structures and Materials, University of Texas at Austin, WRW 110/C0600, Austin, TX 78712-1085, USA

Received 30 January 2001

Abstract

In Part II we examine and evaluate the performance of three levels of models for estimating the two new propagation pressures of pipe-in-pipe systems introduced in Part I (P_{P2} and P_{PS}). The first type of model involves uniform collapse of the system through a kinematically admissible mechanism resulting from the formation of plastic hinges. Closed-form expressions for P_{P2} and P_{PS} are derived which provide a valuable qualitative view on how they depend on the main parameters of the problem. The predictions, however, significantly underpredict the measured values. The second type of model also involves uniform collapse but is conducted numerically instead. An energy balance between prebuckling and collapsed configurations obtained from a uniform collapse model yields approximate values of P_{P2} and P_{PS}. It is demonstrated that such predictions are within acceptable engineering accuracy. The third type of model involves fully three-dimensional numerical simulation of the initiation and steady-state propagation of collapse. It is demonstrated that, provided the geometric and material characteristics of the pipes used are accurately represented in such models, both P_{P2} and P_{PS} can be predicted to great accuracy. Such models are, however, numerically intensive. Part II finishes with conclusions and design recommendations drawn from both the experimental and analytical parts of the study.

Keywords: Propagating collapse; Pipe-in-pipe; Propagation pressure

1. Introduction

In Part I of this two part series of reports, it was demonstrated that pipe-in-pipe systems under external pressure applied to the carrier pipe can develop propagating buckles. The phenomenon is very similar to that known to occur in single pipes. A propagating buckle is initiated when a section of pipe locally weakened by a dent, bending buckle or something else, collapses locally. In the present two-pipe setting, such an event usually will also result in collapse of the inner pipe. Subsequently, provided the external pressure is at a high enough level, the collapse propagates dynamically flattening both pipes as shown in Fig. 4b. [1] The lowest

* Corresponding author. Fax: +1-512-471-5500.
E-mail address: skk@mail.utexas.edu (S. Kyriakides).

[1] Indicates figures, tables and references appearing in Part I.

0020-7683/01/$ - see front matter
PII: S0020-7683(01)00164-0

pressure at which such a buckle will propagate is the propagation pressure of the two-pipe system (P_{P2}). At this pressure the buckle propagates quasi-statically. In Part I this new propagation pressure and its dependence on the problem parameters were examined experimentally.

The experiments demonstrated that as the inner pipe wall increases P_{P2} increases with a quadratic dependence on t_i. If we fix the values of the carrier and inner pipe diameters and properties, for each carrier D/t there is an inner pipe wall thickness beyond which a quasi-statically initiated and propagated buckle tends to only affect the carrier pipe. The buckle propagates over the inner pipe leaving it intact. The pressure at which this occurs corresponds to that of a similar propagation event in a system in which the inner pipe is replaced by a solid rod (P_{PS}). If the wall thickness of the inner pipe is higher than this critical value, once the finite length outer pipe is collapsed, a second quasi-static propagating instability takes place at a pressure higher (usually) than P_{PS}. This time, the inner pipe is collapsed also. It was observed that when this double propagation event took place the inner pipe was not totally collapsed because of its higher wall thickness and stiffness.

In Part II we examine and evaluate the performance of three levels of models for estimating P_{P2} and P_{PS}. The models are similar to those used to predict the propagation pressure of single pipes (P_P) as summarized in Kyriakides (1993).[1] The first type models involve uniform collapse of the systems through kinematically admissible mechanisms resulting from the formation of plastic hinges. The second type also involves uniform collapse but one conducted numerically instead.

The propagation pressures of such uniform collapse models come from approximate energy balance type arguments involving the initial and collapsed configurations. The third type model involves a full numerical simulation of the initiation and steady-state propagation process using finite elements. As was the case for similar calculations for single pipes, the third type model will be shown to yield propagation pressures to high degrees of accuracy. The strengths and weaknesses of the other two types of models will be evaluated by comparison to the experimental results.

2. Uniform collapse models

2.1. Discrete models

The simplest model for estimating the propagation pressure of single pipes is one of the Palmer and Martin (1975).[1] The variation in deformation in the profile of a buckle propagating quasi-statically is neglected. Instead, only the initial and final configurations of the cross-section of the pipe are considered. Furthermore, deformation is limited to four hinges placed as shown in Fig. 1a and the material is assumed to be rigid-perfectly plastic with yield stress σ_o. The plastic work expended in the four hinges is equated to the work done by the pressure due to the change in volume in going from the initial to the collapsed cross-section yielding the following expression for the propagation pressure:

$$\hat{P}_P = \pi\sigma_o\left(\frac{t}{D}\right)^2. \tag{1a}$$

In such 2D approximations of the process, it is preferable to consider instead the pipe to be collapsing under plane strain conditions (Chater and Hutchinson, 1984; Kyriakides et al. (1984b);[1] Kyriakides and Chang, 1992). This changes Eq. (1a) to

$$\hat{P}_P = \frac{2\pi}{\sqrt{3}}\sigma_o\left(\frac{t}{D}\right)^2. \tag{1b}$$

Because of their simplicity the values of P_P predicted by these expressions are only of qualitative value. Although some improvements can be made by making the material model of the hinges more realistic by

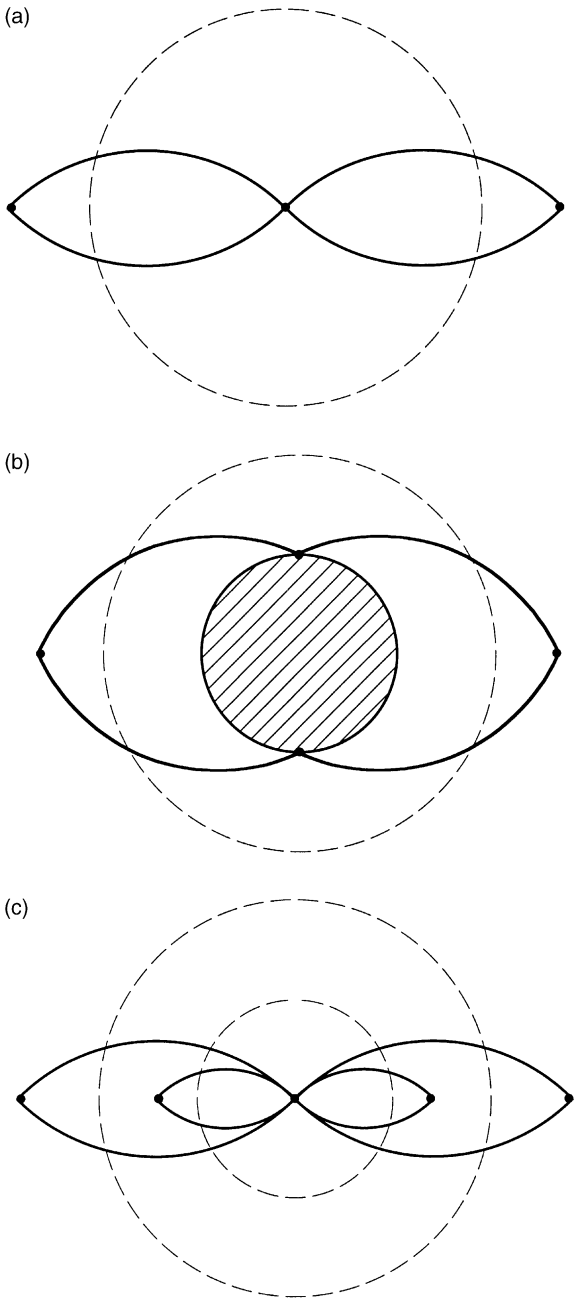

Fig. 1. Discrete models for pipe collapse. (a) Single pipe. (b) Pipe with solid insert. (c) Pipe-in-pipe system.

including strain hardening (e.g. see Kyriakides (1993) [1]) we will extend these models to the present problems in their simpler form as they provide a simple setting for capturing the dependence of the propagation pressures on the main parameters of the problems.

Fig. 1b shows the same four-hinge model but with a solid, circular insert of diameter D_S. The same arguments result in the following expression for the steady-state propagation of collapse over the solid insert

$$\hat{P}_{PS} = \frac{2\pi}{\sqrt{3}}\sigma_o\left(\frac{t}{D}\right)^2\left[\frac{1-\frac{4}{\pi}\phi}{1-\sqrt{2}\left(\frac{D_S}{D}\right)\cos\phi}\right], \tag{2a}$$

where

$$\phi = \cos^{-1}\left[1-\frac{1}{2}\left(\frac{D_S}{D}\right)^2\right]^{1/2}, \quad 0 \leqslant \phi < \frac{\pi}{4}. \tag{2b}$$

In the limit when $D_S = 0$ Eqs. (2a) and (2b) reduces to Eq. (1b).

As is the case for Eqs. (1a) and (1b) for the single pipe, the actual numerical values of Eqs. (2a) and (2b) underpredict the experimental results significantly. The extent can be seen in Table 3 where results from several models are presented along with corresponding experimental results. One way of making these equations more representative of reality is to normalize $\hat{P}_{PS}$ by the value of $\hat{P}_P$ yielded when $D_S = 0$ (i.e. Eq. (1b)—a similar approach was used by Kyriakides and Chang (1992) for a related problem). Fig. 2 shows a comparison of the experimental results with the results of this model normalized in this manner. The powerlaw dependence on D_S/D seen in the experiments is captured by the model but with a different exponent. As a result, the predictions now seemingly overestimate the experimental results.

Fig. 1c shows the four-hinge mechanisms applied to a pipe-in-pipe system. The calculation is similar except that now the internal work expended in the hinges of the inner pipe must be included. As with the models above, the assumption that the walls of the cross-sections are thin is adhered to for simplicity. The following expression for the propagation pressure is derived

$$\hat{P}_{P2} = \frac{2\pi}{\sqrt{3}}\sigma_o\left(\frac{t}{D}\right)^2\left[1+\frac{\sigma_{oi}}{\sigma_o}\left(\frac{t_i}{t}\right)^2\right], \tag{3}$$

where the term outside the square bracket represents the propagation pressure of the carrier pipe alone. Interestingly, the quadratic dependence on the thickness ratio of the two pipes seen in the experiments is captured (see Eq. (6) in Part I). The dependence on the yield stress ratio is also captured but with an exponent of 1. The dependence on the diameter ratio is not captured partly because we neglected the effect of the finite wall thickness of the two pipes. Numerical values yielded by this expression for specific cases are

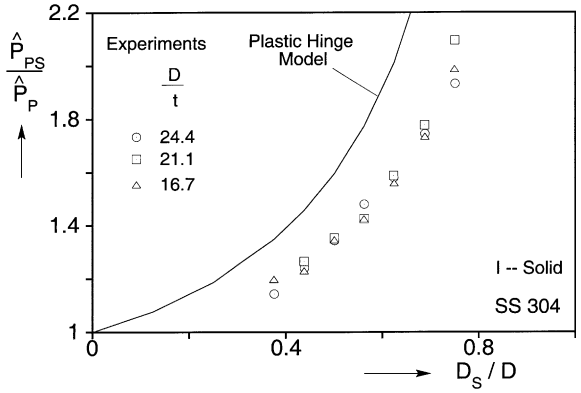

Fig. 2. Propagation pressure of tubes with solid inserts and prediction from plastic hinge model.

included in Table 3. They are seen to underpredict the experimental results. Some improvement in expressions (1)–(3) can be achieved by making the material model more realistic by including the post-yield behavior of the material. Guidance on how this can be achieved is given in Kyriakides (1993).[1] Alternatively, improved schemes such as those of Wierzbicki and Bhat (1986) or Kamalarasa and Calladine (1988) which include the effect of axial deformation can be considered.

2.2. Numerical models

The same 2D calculations are now repeated using finite elements. Such models were first used by Kyriakides and Babcock (1981) to gain insight into the initiation and steady-state propagation of buckles in single pipes. The models were extended in Chater and Hutchinson (1984) and Kyriakides et al. (1984a)[1] by using an energy balance to produce an improved estimate of P_P (see also Kyriakides and Arikan (1983)). The advantage these models have over full three-dimensional (3D) models is their efficiency. They are, however, approximate in nature and, as shown in the comparative study of Dyau and Kyriakides (1993b),[1] become progressively less accurate as the D/t of the pipe analyzed decreases. The present models were developed within the FE code ABAQUS. The rings were collapsed under plane strain conditions. Thickness variations were neglected and thus the models were symmetric about two orthogonal axes passing through their common center. As a result, only one-quarter of the cross-sections was analyzed. The rings were discretized with 8-node quadratic plane strain elements with full integration (CPE8). Eight elements were used through the thickness of each ring and 40 around the circumference. Convergence studies showed this distribution to be excessive. It was however not changed because of the relative numerical efficiency of such 2D calculations.

Contact between the surfaces of the outer and inner rings was treated using contact surfaces with "arbitrary" sliding. The inner ring's deformation was limited by a rigid surface placed along the appropriate plane of symmetry. The solid insert was modeled as a circular cylindrical rigid surface.

The material was modeled as a finitely deforming J_2-type elastic plastic solid which hardens isotropically. A measured true stress–logarithmic strain response is shown in Fig. 3. The shape was kept the same but the yield stress was adjusted to correspond to the value representative of the experiment(s) simulated. In all cases a small initial imperfection in the form of initial ovality $(w_o = (\Delta_o D \cos 2\theta)/2)$ with an amplitude of 0.4% was introduced to the carrier tube in order to help induce collapse. Loading was accomplished by the use of hydrostatic fluid elements placed on the exterior of the carrier tube. This enables incremental prescription of the volume of fluid in an imaginary cavity surrounding the tube.

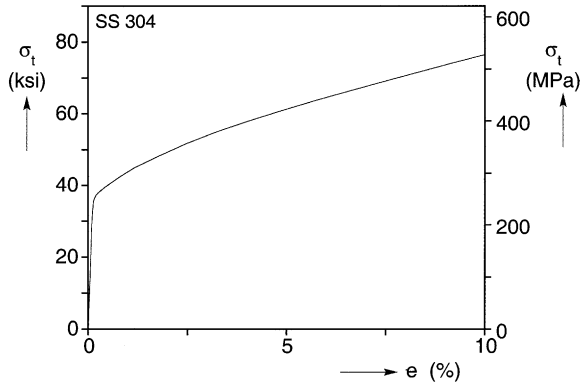

Fig. 3. True stress–logarithmic strain response typical of material analyzed.

Table 1
Geometric and mechanical properties of tubes with solid inserts used in the 2D models

D/t	D (mm)	t (mm)	σ_o ksi (MPa)	S	$\overline{P}_P$ psi (bar)
24.01	1.998 (50.75)	0.0832 (2.11)	47.51 (327.7)	0.92	618 (42.6)
21.28	2.001 (50.82)	0.0940 (2.39)	41.06 (263.2)	1.0	778 (53.7)
16.64	2.000 (50.80)	0.1202 (3.05)	49.95 (344.5)	0.885	1584 (109.3)

2.2.1. Solid inserts

We first consider results for tubes with solid inserts. In these calculations we use the average geometric and material properties of each set of tubes used in the corresponding experiments which are listed in Table 1. A typical pressure-change in volume response for a carrier tube with $D/t = 24.1$ and a solid insert with $D_S = 0.56D$ is shown in Fig. 4a. The pressure is normalized with the mean value of the measured propagation pressures of the tubes used in the corresponding experiments ($\overline{P}_P$ in Table 1). The change in external volume (Δv) is normalized by the initial volume of a unit length of the tube (v_o). The initial (⓪) and a set of four deformed configurations corresponding to the points marked on the response with numbered flags are shown in Fig. 4b. The response traces an *up–down–up* trajectory characteristic of systems which have the potential of developing a propagating instability. The first pressure maximum represents the collapse pressure of the tube. The collapse pressure depends on the tube geometric and material parameters including the initial ovality. Accuracy in the predicted collapse pressure is not important in what follows and thus the arbitrariness of the value of $\Delta_o = 0.004$ adopted is acceptable. Beyond the pressure maximum the tube collapses with decreasing pressure (see configurations ①, ② and ③ in Fig. 4b). By configuration ③ the walls of the ring come into contact with the solid rod and the structure is stabilized as indicated by the sharp rise in pressure. Eventually the four quadrants of the cross-section which act somewhat like arches become further plasticized by membrane action and a pressure maximum develops indicating the development of a new collapse mechanism (see ④). This is of no interest to us and will not be pursued further.

The first ascending branch of this up–down–up response represents stable, essentially elastic prebuckling configurations. The descending branch represent unstable configurations and the second ascending branch stable, plasticized collapsed configurations. An estimate of the propagation pressure of the system is obtained by conducting an energy balance between configurations like A on the first ascending branch and C on the second (Chater and Hutchinson, 1984; Kyriakides et al., 1984b [1]). We argue that configuration C can be reached either by following the up–down–up response or by steady-state propagation at a pressure corresponding to the level of ABC. If the material behavior is path independent, the difference in the internal energy of the two states in the two processes is the same. In the latter process the work done by the constant pressure is

$$\hat{P}_{PS}(\Delta v_C - \Delta v_A). \tag{4a}$$

When this is equated to the difference in internal energy between configurations A and C the following expression for the propagation pressure is obtained:

$$\hat{P}_{PS} = \frac{1}{(\Delta v_C - \Delta v_A)} \int_{\Delta v_A}^{\Delta v_C} P(\Delta v)\, d\Delta v. \tag{4b}$$

This requires that ABC be at a level that makes the areas under the response above the line and below it equal (*Maxwell* pressure) as shown in Fig. 4a. For this class of problems, a weakness in this argument is that the elastoplastic material of the deforming carrier tube is path dependent which introduces an error in the predicted propagation pressure. In this case the predicted value is $\hat{P}_{PS} = 1.2265\overline{P}_P$ which compares to the experimental value of $1.480P_P$ (albeit with slightly different properties—see Table 4a [1]). Kyriakides

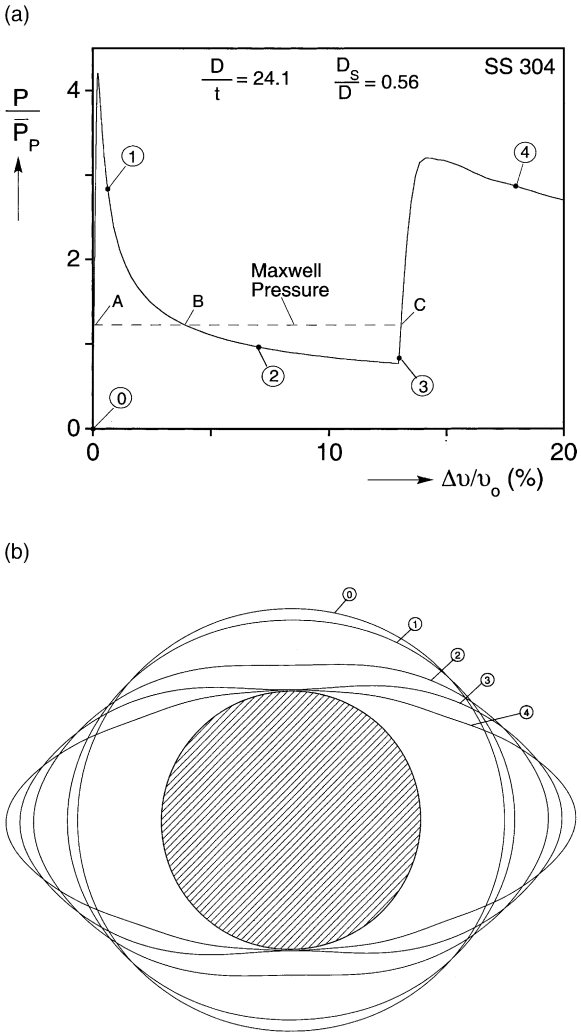

Fig. 4. Uniform collapse of tube with solid insert. (a) Pressure-change in volume response. (b) Sequence of collapse configurations corresponding to (a).

et al. (1984b)[1] and, in more detail, Dyau and Kyriakides (1993b)[1] showed that for single pipes this error tends to increase as the D/t becomes lower because of the increase in inelastic action.

Similar calculations were performed for the same carrier tube and solid inserts with the same diameters as those used in the experiments. The calculated responses are shown in Fig. 5. The base response is that of the carrier tube alone ($D_S = 0$). The second ascending branch of each case with a solid insert is nearly vertical and intersects the base response when the inner surface of the collapsing tube contacts the rod. Thus, provided the displacement of the crown point is monitored appropriately, the response of the carrier pipe alone can suffice and the second ascending branch can be established approximately by constructing a vertical line at the point corresponding to first contact with the solid rod.

Fig. 6 shows a comparison of the measured and predicted values of P_{PS} for various values of D_S/D. The experimental values of P_{PS} are normalized by the measured propagation pressures of the carrier tubes (see Table 4a[1]) used whereas the predicted values are normalized by the mean value $\overline{P}_P$ listed in Table 1. As

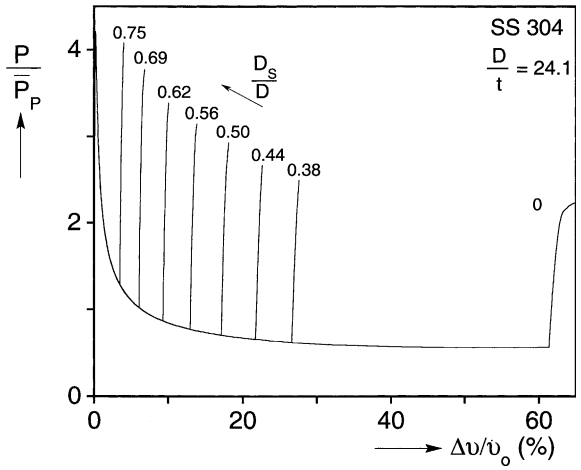

Fig. 5. Pressure-change in volume responses for uniform collapse of carrier tube with $D/t = 24.1$ and solid inserts of various diameters.

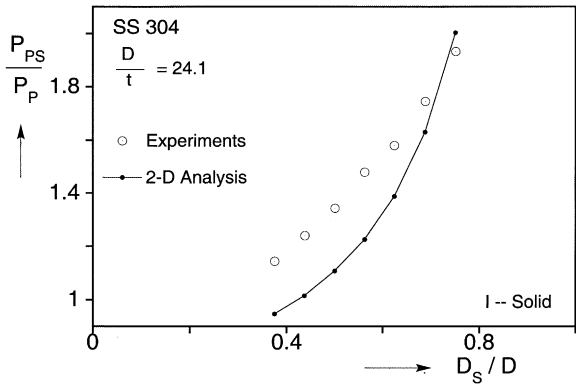

Fig. 6. Comparison of measured and predicted P_{PS} values for carrier tube with $D/t = 24.1$.

expected, the propagation pressure predicted for this tube by this type model is 26.2% lower than the mean value measured in the experiments. For cases with solid inserts, the analytical results underpredict most of the experimental values but the difference between the two decreases as the diameter of the solid insert increases. This can be attributed to the decrease in inelastic action resulting from the more limited deformation of the collapsing carrier tube for larger values of D_S. In fact, for the largest solid rod diameter considered ($D_S/D = 0.75$) the predicted P_{PS} is slightly higher than the measured value.

Similar sets of calculations were conducted for the other two carrier tube families used in the experiments. Figs. 7 and 8 show comparisons of measured and predicted values of P_{PS} as a function of D_S/D for D/t values of 21.1 and 16.7 respectively. As expected, the difference between the predicted and measured value of P_P increases as the D/t becomes lower. The predicted values were 27.3% lower than $\overline{P}_P$ in Table 1 for $D/t = 21.1$ and 30.5% lower for 16.7. In the presence of the solid inserts the difference shows the same decreasing trend with D_S as the results in Fig. 6 but, generally, the deviation increases as the D/t becomes lower. Overall, based on the results we can conclude that, provided the solid insert diameter is larger than $0.5D$, this type 2D model can yield engineering accuracy predictions of P_{PS}. The predictions becoming increasingly of higher accuracy as the diameter of the solid rod increases. In view of the importance of P_{PS} in

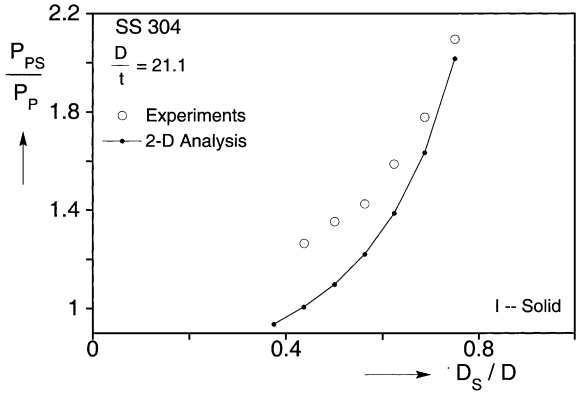

Fig. 7. Comparison of measured and predicted P_{PS} values for carrier tube with $D/t = 21.1$.

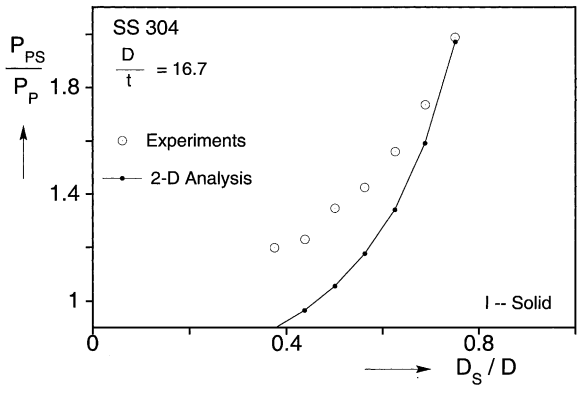

Fig. 8. Comparison of measured and predicted P_{PS} values for carrier tube with $D/t = 16.7$.

the design of pipe-in-pipe systems alluded to in Part I, this conclusion is a useful tip because of the relative efficiency of this calculation.

2.2.2. Pipe-in-pipe systems

We now turn to results from similar calculations for pipe-in-pipe systems. The initial detailed discussion will be around results from carrier tubes with $D/t = 21.1$. These results are based on average geometric and material properties of such tubes used in experiments with $D_i/D = 0.624$ listed in Table 2. The first $P - \Delta v$ response shown in Fig. 9a is from a two ring system with an inner ring of $D_i/t_i = 25.53$. The calculated pressure is normalized by $\overline{P}_P = 756$ psi (52.1 bar) which represents the mean value of the measured propagation pressure of the carrier tubes tested in this group. Fig. 9b shows the initial and a set of deformed configurations corresponding to the points marked by solid bullets on the response. The initial part of the response represents the initial collapse of the carrier tube and is similar in all respects to the ones presented for the solid inserts (e.g., ①). The collapse is arrested when the outer ring contacts the inner one (②) and the response returns to positive slope once more. This increase in pressure causes the two rings to start deforming together. As the inner ring becomes plasticized the response becomes less stiff and, soon thereafter, a new local pressure maximum develops. Subsequently, the two rings collapse together with a decreasing pressure (see ③ and ④). The next major change in behavior occurs when the walls of the inner ring come

Table 2
Geometric and mechanical properties of pipe-in-pipe systems used in the 2D models

D/t	D (mm)	t (mm)	σ_o ksi (MPa)	S	$\overline{P}_P$ psi (bar)	D_i (mm)	σ_{oi} ksi (MPa)
24.11	2.000 (50.79)	0.0829 (2.11)	41.19 (284.1)	0.894	553 (38.1)	1.251 (31.77)	55.30 (381.4)
21.50	2.004 (50.90)	0.0932 (2.37)	40.09 (276.5)	1.0	756 (52.1)	1.251 (31.78)	46.96 (323.9)
16.68	2.000 (50.80)	0.1199 (3.05)	46.60 (321.4)	0.925	1551 (106.9)	1.251 (31.78)	45.28 (312.3)

into contact (⑤). This stabilizes the response once more resulting in the nearly vertical trajectory shown in the figure. Very much as is the case for single rings, the response starts to lose stiffness at high pressures when the arch-like quadrants get plasticized by high membrane stresses and eventually collapse. These events go beyond our present needs and will not be pursued.

Despite the two wells in this response the estimation of the propagation pressure follows the same lines as described above. The Maxwell pressure, marked with a dashed line in Fig. 9a, is at $0.9815\overline{P}_P$ which is on the order of 17% lower than the experimental value.

Fig. 10a shows a similar $P-\Delta v$ response for a somewhat thicker inner ring ($D_i/t_i = 19.25$) and Fig. 10b shows a set of deformed configurations corresponding to it. The response is similar but the depth of the first well has increased because of the increased resistance from the inner tube. As a result, a separate Maxwell pressure can now be established for the first well at the level of $1.336\overline{P}_P$. This is within 1% of the pressure that corresponds to $\hat{P}_{PS}$ yielded by this 2D model for this carrier tube. Thus, the model predicts that collapse can propagate with the inner tube staying intact (configuration ③).

Two more Maxwell pressures can be calculated for this case. Using the whole response yields a Maxwell pressure of $1.222\overline{P}_P$. A third value at the level of $1.198\overline{P}_P$ is yielded by using only the second pressure well. These can be interpreted as follows. The lower of the two can be viewed as the pressure at which collapse will propagate following first propagation over the inner tube at $1.336\overline{P}_P$. In other words, the two events would occur sequentially. The Maxwell pressure corresponding to the whole response is the pressure level at which collapse will propagate collapsing both tubes simultaneously. In practice this is possible by indenting both tubes sufficiently. Since the combined collapse propagation pressure is lower than the pressure corresponding to collapse over the inner tube the lower value should prevail. This three propagation pressure scenario is rare. A two-propagation pressure scenario like the one for the case that follows was more common in the experiments.

Fig. 11a shows the $P-\Delta v$ response corresponding to an even thicker inner tube with $D_i/t_i = 15.07$. The depth of the first well has increased further but the Maxwell pressure corresponding to it has increased only slightly to $1.345\overline{P}_P$ which is even closer to the corresponding solid insert value. This of course reflects the increased rigidity of the inner tube. A second Maxwell pressure is yielded by the second pressure well at the higher level of $1.638\overline{P}_P$. In this case no ambiguity as to what can be expected is present. A two-propagation scenario is predicted; the first is at $1.345\overline{P}_P$ followed by the second at $1.638\overline{P}_P$. Fig. 11b shows a sequence of deformed configurations corresponding to this response. Configuration ③ corresponds to the first propagation event which leaves the inner tube intact. Configuration ⑤ corresponds to the second propagation event following the first. The inner tube now deforms but its walls do not come into contact as was observed in several of the experiments.

Similar calculations were performed for several other inner tube geometries. The calculated responses are shown in Fig. 12 (without the Maxwell constructions). The predicted propagation pressures normalized by $\overline{P}_P$ are plotted against the inner ring thickness normalized by t in Fig. 13. In cases where two-propagation

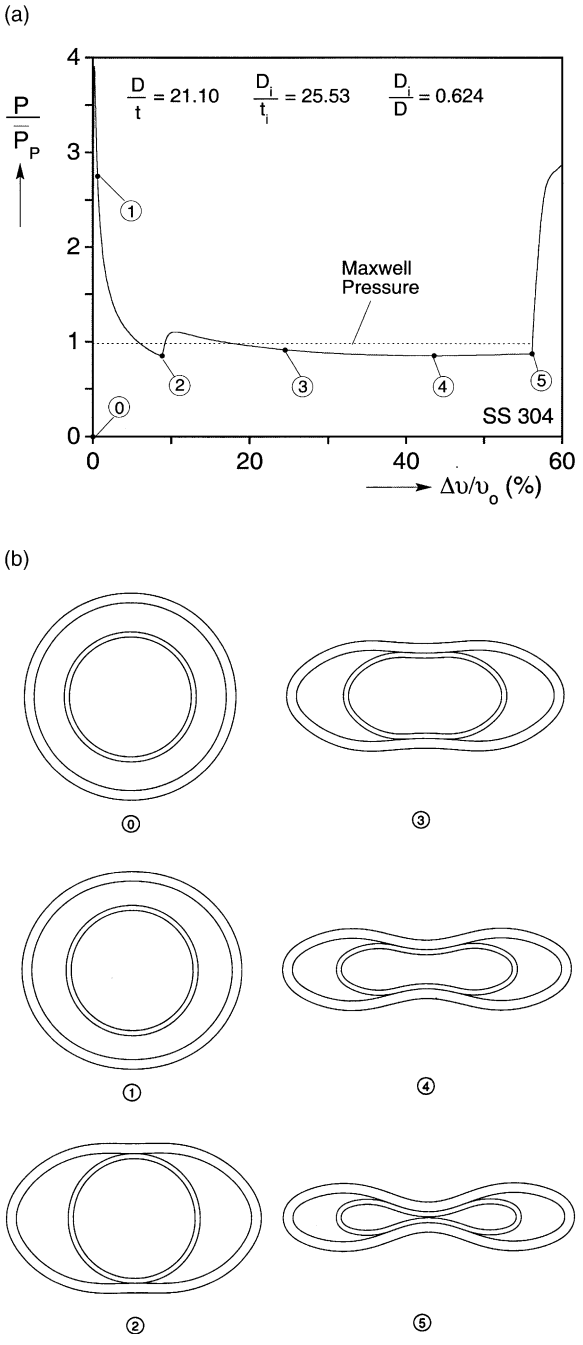

Fig. 9. Uniform collapse of tube-in-tube system. (a) Pressure-change in volume response ($D_i/t_i = 25.53$). (b) Sequence of collapse configurations corresponding to (a).

pressures were predicted the second one was adopted as was done in the experiments. The seven experimental points in this set are also included in the figure as are the measured and predicted P_{PS}/P_P values. As

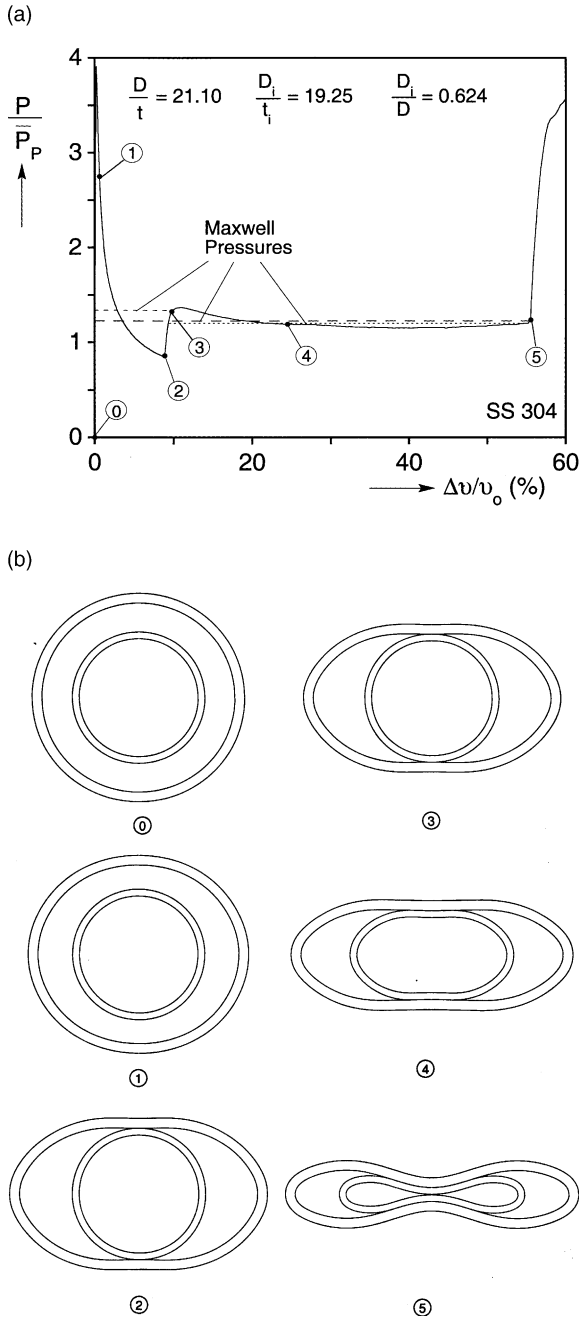

Fig. 10. Uniform collapse of tube-in-tube system. (a) Pressure-change in volume response ($D_i/t_i = 19.25$). (b) Sequence of collapse configurations corresponding to (a).

expected, the propagation pressure predicted for the carrier tube alone is 29% lower than the experimental value. $\hat{P}_{P2}$ for the thinnest of the inner tubes differs from the measured value by somewhat more than 30%. This discrepancy decreases for thicker inner tubes. In fact, for the two thickest inner tubes the model

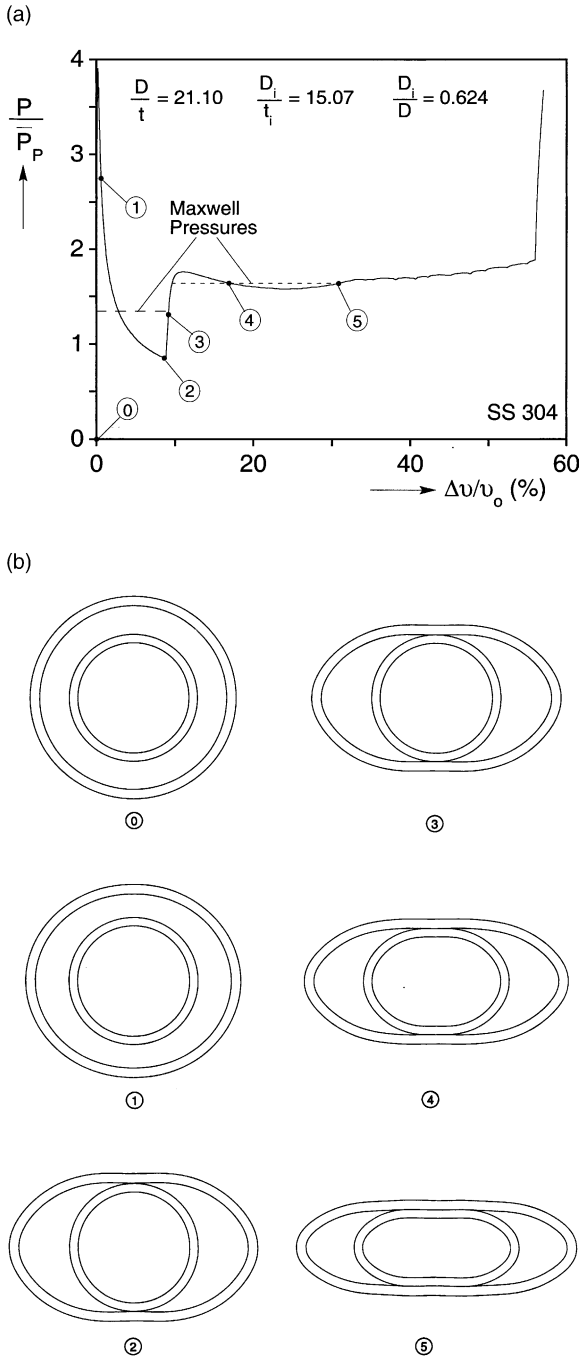

Fig. 11. Uniform collapse of tube-in-tube system. (a) Pressure-change in volume response ($D_i/t_i = 15.07$). (b) Sequence of collapse configurations corresponding to (a).

overestimates the experimental values slightly. The predicted value for P_{PS} is about 17% lower than the experimental value. Because of this, the predicted thickness ratio at which two-propagation pressures

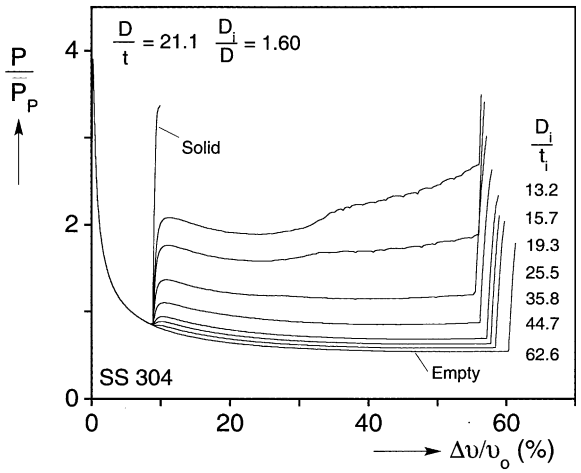

Fig. 12. Pressure-change in volume responses for uniform collapse of carrier tube with $D/t = 21.1$ and inner tubes of $D_i/D = 1.60$ and various values of wall thickness (t_i).

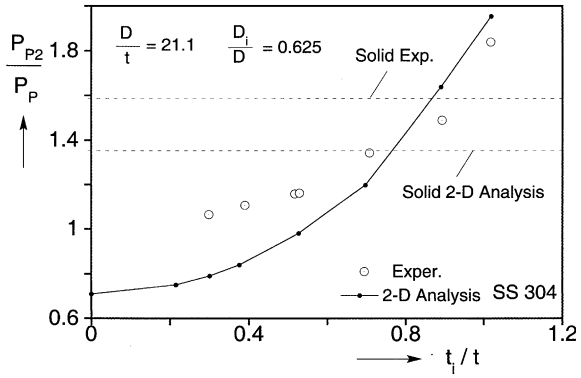

Fig. 13. Comparison of measured and predicted P_{P2} values for carrier tube with $D/t = 21.1$.

become possible is lower than the actual value. Thus, for example, for the case with $D_i/t_i = 19.25$ presented in Fig. 10 the multiple propagation phenomena predicted did not materialize in practice. In the experiment only one-propagation pressure could be established.

Similar calculations were performed for one of the sets of experiments performed on carrier tubes with $D/t = 24.1$ and for one set with $D/t = 16.7$. The parameters used in these calculations are listed in Table 2. The calculated P_{P2} values for carrier tubes with $D/t = 24.1$ normalized by $\overline{P}_P$ given in Table 2 are plotted against t_i/t in Fig. 14. Included in the figure are the corresponding experimental values as well as the predicted and measured P_{PS}/P_P values. The trend in the results is similar to what was observed for $D/t = 21.1$. For thinner inner tubes, the predicted propagation pressures are lower than the measured values. For thicker inner tubes, the difference is smaller and, for the thickest case considered, the prediction is higher than the experimental value. This is related to the fact that the extent of cross-sectional deformation at the propagation pressure decreases as the ring wall thickness is increased. Indeed, as we saw for thicker rings, the walls of the inner ring never come into contact. Again, the predicted value of P_{PS} is lower

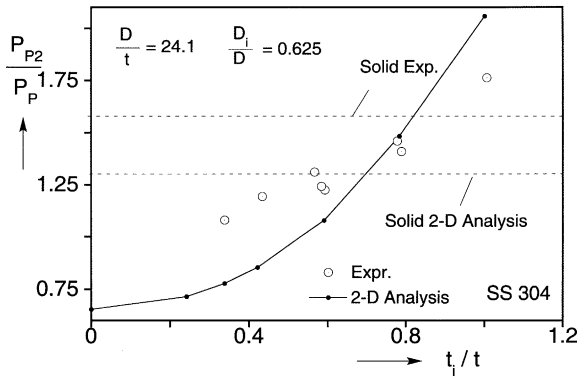

Fig. 14. Comparison of measured and predicted P_{P2} values for carrier tube with $D/t = 24.1$.

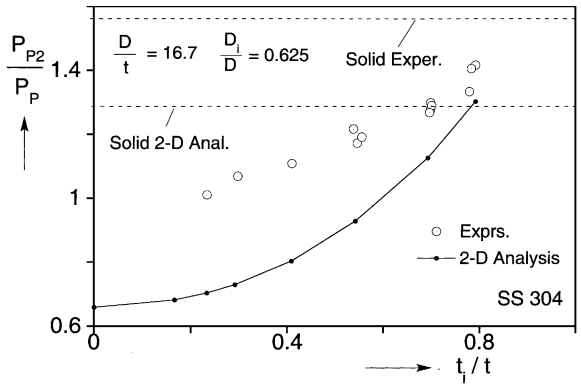

Fig. 15. Comparison of measured and predicted P_{P2} values for carrier tube with $D/t = 16.7$.

than the measured value and, as a result, the predicted transitional value of t_i/t for switching from single to multiple propagation pressures is somewhat low.

Fig. 15 shows a similar comparison of experimental results and 2D predictions for $D/t = 16.7$. In this case all inner tube wall thicknesses examined are thinner than the wall of the carrier tube. Thus, the collapse of the carrier tube dominates the process resulting in contact of the inner tube walls at propagation in all cases examined. Furthermore, in all cases the propagation pressures remained below P_{PS}. For these reasons the predicted values of P_{P2} are generally lower than the experimental values. Again the difference between predictions and experiments decreases as t_i increases.

In summary, the 2D models are attractive because of their relative numerical efficiency. For the pipe parameters used in this study, the predicted propagation pressures for pipe-in-pipe systems are generally lower than measured values although the predictions approach the experimental results for thicker inner tubes. Overall, for the parameters used in this study P_{P2} was predicted to within acceptable engineering accuracy. Thus, such models could be used to study the parametric dependence of P_{P2} to generate design charts. The models also reproduce qualitatively the multiple collapse propagation phenomena discovered in the experiments. The transitional value of t_i/t at which they start to occur is underestimated however.

3. Full scale numerical simulation of buckle propagation

In their comparative study of models for calculating the propagation pressure of single pipes, Dyau and Kyriakides (1993b)[1] clearly illustrated that the most dependable way of predicting this critical pressure of pipelines is a full 3D numerical simulation of the process of initiation and steady-state propagation of collapse (for alternate 3D numerical simulations of steady-state buckle propagation see Jensen (1988) and Nogueira and Tassoulas (1994)). The process is similar to the experimental procedure through which propagation pressure is usually established. It was demonstrated that, provided the geometry of the pipes and the material inelastic behavior are modeled appropriately, the propagation pressure can be predicted to excellent accuracy. The Dyau and Kyriakides model was based on the principle of virtual work and the structure was discretized with global functions. In similar studies that followed involving integral buckle arrestors, finite elements were used to discretize the structures because of the flexibility they provide and the more robust numerical procedures available for handling them (Park and Kyriakides, 1997;[1] Netto and Kyriakides, 2000). In the present study the FE framework of these references is adopted and extended to the needs of the two-pipe systems of interest.

The models are again developed within the FE code ABAQUS/5.8. For the cases that will be discussed, the individual geometric and material characteristics of tubes used in specific experiments will be adopted. Guided by the pipe deformation seen in the experiments, planes 1–2 and 1–3 are assumed to be planes of symmetry (see Fig. 16). Furthermore, as in our past models of related problems (see references given above), we place a local imperfection in the neighborhood of $x_1 = 0$ and assume that plane 2–3 is also a plane of symmetry. This is a convenient way of initiating local collapse which does not affect the subsequent propagation of the buckle. With these symmetries just one-eighth of the domain needs to be modeled. The

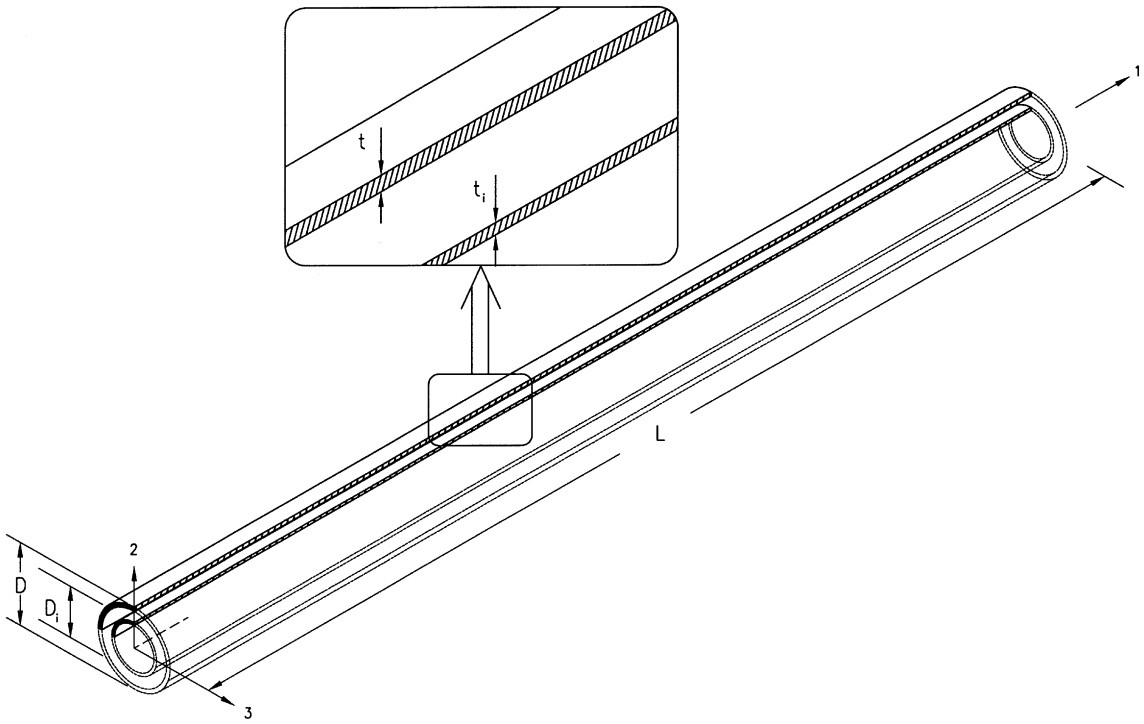

Fig. 16. Geometry of pipe-in-pipe section analyzed in 3D models.

length (L) of the section considered was $10D$. The carrier tube is assumed to have "fixed" boundary conditions at $x_1 = L$ but it is free to expand in the x_1-direction. The tubes are assumed to be circular and the wall thicknesses to be uniform. The local imperfection has the form of

$$w_o(\theta) = -\Delta_o\left(\frac{D}{2}\right)\exp\left[-\beta\left(\frac{x_1}{D}\right)^2\right]\cos 2\theta, \tag{5}$$

where w_o is the radial displacement and θ the polar angular coordinate measured from x_2. The amplitude of the imperfection is Δ_o (=0.004) and β decides its extent which typically will be $0.5D$ long.

The two tubes are discretized in the same manner using 240 3D, 27-node quadratic brick elements with reduced integration (C3D27R) for each. Two elements are used through the thickness of the tubes and the domains are divided into 10 sectors of equal length along the axial direction. Twelve elements are used for each tube in the circumferential direction with the following angular spans starting from the x_2-axis: 2.5–5–5–7.5–15–15–10–10–7.5–7.5–2.5–2.5°.

Since only one-quarter of the model is analyzed, a rigid surface is placed along the symmetry plane 1–3 using rigid elements (R3D4) to simulate contact of the inner walls of the pipe during propagation of collapse. A small-sliding surface-based formulation is used for contact between the pipe and the rigid flat surface. A different formulation is used for contact between the inner and outer pipes. Since displacements (and thus sliding) in the axial direction are expected to be small, circumferential slide lines defined with three node elements (ISL22T) are used. The slide-line formulation is more efficient than surface-based contact for this situation. For cases in which the inner tube is replaced with a rigid rod, a rigid cylinder of the appropriate size is defined, and surface-based contact is used between the outer tube and the rigid cylinder.

As in past similar calculations, a "volume controlled" loading procedure is adopted using the hydrostatic fluid elements of ABAQUS (a combination of F3D3 and F3D4). These elements allow prescription of the change in volume inside a control region defined around the structure. The pressure becomes an additional unknown while the volume change becomes a constraint via the Lagrange multipliers method.

The materials of the pipes and arrestors are modeled as J_2-type, elastoplastic, finitely deforming solids which harden isotropically. The anisotropic yielding observed in the experiments is treated through Hill's anisotropic yield function (Hill, 1948). It is assumed that the through-thickness and transverse yield stresses are the same but generally lower than the yield stress in the axial direction by the factor S established in the experiments. The models are calibrated to piecewise linear approximations of the true stress–logarithmic strain versions of the measured stress–strain responses of the tube materials.

3.1. Propagation of collapse in a single pipe

For completeness we first consider a simulation of the initiation and propagation of collapse under quasi-static conditions in a single tube. The main parameters of the tube used are listed in Table 3 (Exp. 18—this tube came from the same length that the section used in Exp. 21 originated—see Table 1 [1]). Fig. 17a shows the calculated pressure change in volume response, and Fig. 17b shows the initial and four deformed configurations corresponding to the points marked on the response with numbered flags. In order to maintain consistency in the presentation of results with pipe-in-pipe and pipe-solid insert cases that follow, configurations show one-quarter of the deforming cross-section (cut made along plane x_1–x_2). The pressure is normalized by the calculated collapse pressure of the intact tube ($\hat{P}_{CO}$ given in Table 3). The response exhibits an initial stable part which is terminated by a pressure maximum. This corresponds to the collapse pressure of the specimen which is affected by the amplitude and extent of the local imperfection introduced in the neighborhood of $x_1 = 0$ for the purpose of initiating collapse. In general, the pressure maximum is somewhat smaller than P_{CO} because actual imperfections are smaller than the value assumed in the calculations. Following the pressure maximum, collapse localizes as illustrated by configurations ① and ②

Table 3
Comparison of measured and predicted propagation pressures

Tube parameters								$\hat{P}_{P2}$ psi (bar)				
Exp. no.	D (mm)	D/t	σ_o ksi (MPa)	D_i (mm)	D_i/t_i	σ_{oi} ksi (MPa)	$\hat{P}_{CO}$ psi (bar)	PH model	2D model	3D model	Exp.	Diff. (%)
18	2.000 (50.80)	21.10	38.2 (263)	–	–	–	2709 (186.7)	239 (16.5)	381 (26.3)	531 (36.6)	532 (36.7)	−0.2
19	2.000 (50.80)	24.10	38.2 (263)	1.248 (31.67)	–	–	2709 (186.7)	480 (33.1)	719 (49.6)	850 (58.6)	841 (58.0)	1.1
51	1.999 (50.77)	24.04	40.73 (281)	1.249 (31.72)	19.07	40.28 (278)	2368 (163.3)	412 (28.4)	708 (48.8)	710 (49.0)	717 (49.4)	−1
53	2.002 (50.85)	24.10	39.63 (273)	1.374 (34.90)	21.57	55.35 (382)	2350 (162.1)	451 (31.1)	713 (49.2)	790 (54.5)	778 (53.7)	1.5
74	1.999 (50.77)	21.77	41.95 (289)	1.250 (31.75)	13.33	34.60 (239)	2778 (191.6)	597 (41.2)	887 (61.2) 1232 (85.0)	1096 (75.6) 1255 (86.6)	1115 (77.8) 1220 (84.1)	−1.7 2.9
13	1.999 (50.77)	16.69	53.5 (369)	1.248 (31.67)	–	–	5485 (378.3)	1402 (96.7)	2184 (150.6)	2583 (178.1)	2583 (178.1)	0
52	2.001 (50.83)	16.60	42.54 (293)	1.251 (31.77)	19.01	40.28 (278)	4752 (327.7)	718 (49.5)	1505 (103.8)	1860 (128.3)	1757 (121.2)	5.9
23	1.999 (50.77)	16.60	50.18 (346)	1.373 (34.87)	21.62	55.35 (382)	5108 (352.3)	848 (58.5)	1526 (105.2)	1920 (132.4)	1905 (131.4)	0.8

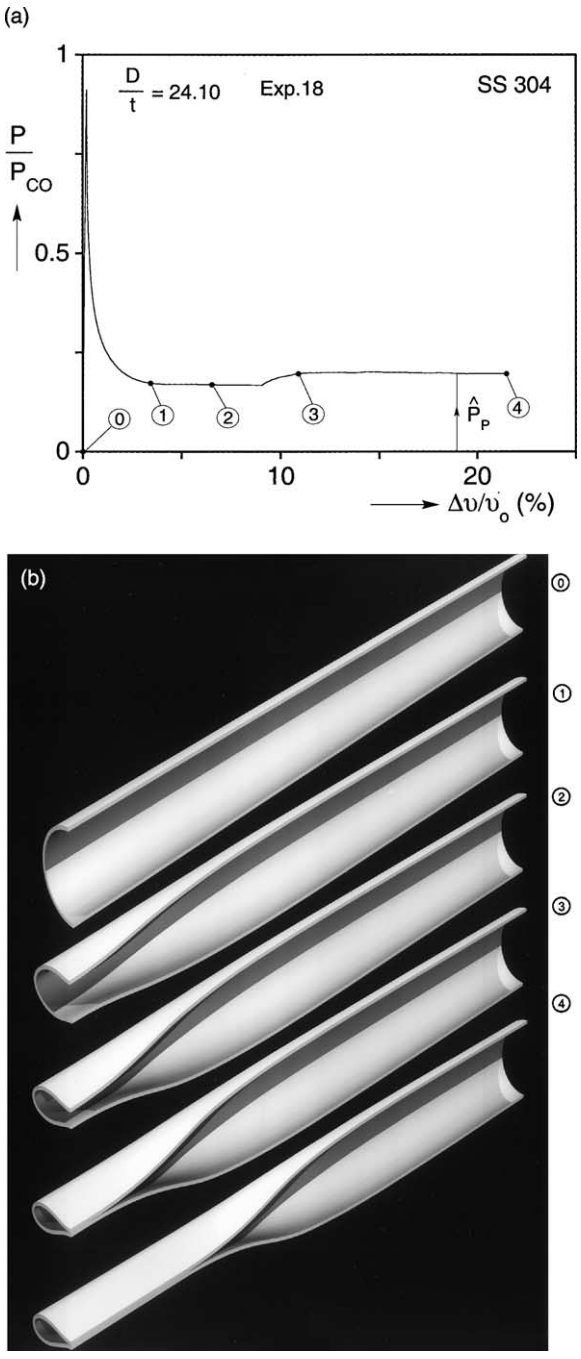

Fig. 17. (a) Calculated pressure-change in volume response for single pipe simulating Exp. 18. (b) Sequence of collapse configurations corresponding to (a).

while the pressure drops precipitously. Shortly after configuration ②, the walls of the collapsing tube come into contact and radial collapse is arrested. This is accompanied with a small increase in the recorded

pressure. By configuration ③ steady-state spreading of collapse down the length of the tube has been achieved and continues in configuration ④ when the calculation was terminated. The pressure plateau traced represents the calculated propagation pressure ($\hat{P}_P$). It is at a level of 531 psi (36.6 bar) which compares with the value of 532 psi (36.7 bar) recorded in the experiment. This level of agreement is typical in such calculations. Table 3 includes predictions of P_P yielded by the corresponding 2D model and by the plastic hinge model (Eq. (1b)). The 2D model underpredicts the experimental value by 28.5% while the prediction of Eq. (1b) is only 45% of the experimental value. Both results support the comments made earlier about the performance of these uniform collapse models.

3.2. Propagation of collapse over solid inserts

We now consider 3D simulations involving pipes with solid inserts. Fig. 18a shows the calculated $P-\Delta v$ response for Exp. 13. The carrier tube has $D/t = 16.69$ and the diameter of the solid insert is $0.624D$. The rest of the parameters of the problem are listed in Table 3. Fig. 18b shows a set of deformed configurations corresponding to points marked on the response. The main characteristic of the calculated response are similar to that exhibited by most propagating instabilities in structures. The carrier tube collapses locally in the neighborhood of the initial imperfection. As was observed in the experiments involving solid inserts in Part I, the solid insert is contacted with relatively small change in volume (compare values of the ordinate—$\Delta v/v_o$— in Figs. 17b and 18b). The solid rod is contacted, radial collapse is arrested and collapse starts to spread along the axis of the tube. The pressure increase between first contact of the solid rod and attainment of steady-state propagation is significantly larger than what is usually observed for similar calculations involving single pipes. This detail was also observed in the experiments (e.g. see Fig. 5[1]). Configuration ① is close to the onset of the pressure plateau that corresponds to $\hat{P}_{PS}$. In configurations ②–④ collapse is propagating in a steady-state manner along the length of the tube.

The predicted value of $\hat{P}_{PS}$ is 2583 psi (178.1 bar) which is exactly coincident with the measured value. By contrast, the corresponding prediction from the 2D model was 15.5% lower than the experimental value. The prediction using Eqs. (2a) and (2b) is at 54% of the measured value.

A second simulation was performed involving a solid insert with $D_S/D = 0.625$ in a carrier tube with $D/t = 24.1$. The data is given in Table 3 and corresponds to Exp. 19. The predicted $\hat{P}_{PS}$ is 850 psi (58.6 bar) or 1.1% higher than the measured value. The corresponding prediction from the 2D model is 14.5% lower than the measured value while Eqs. (2a) and (2b) yields a propagation pressure which is only 57% of the measured value. Overall, the predictions from the 3D model are once again excellent; those from the 2D model are within engineering accuracy and those from the plastic hinge model are of qualitative value.

3.3. Propagation of collapse in pipe-in-pipe systems

3D simulations were also performed for pipe-in-pipe systems. Fig. 19a shows the calculated $P-\Delta v$ response for Exp. 53. The carrier tube has $D/t = 24.1$ and the inner tube has a diameter of $0.687D$ and $D_i/t_i = 21.57$. Other parameters of the problem are listed in Table 3. Fig. 19b shows a set of deformed configurations corresponding to points marked on the response. The initial collapse of the carrier tube is similar to what was described for the cases presented above. Local collapse is temporarily arrested when the inner tube is first contacted. This is reflected by the small increase in the recorded pressure. The inner tube gets quickly plasticized and collapse continues now affecting both tubes as seen in configurations ① and ①. When the walls of the inner tube contact each other, radial collapse is arrested and collapse starts to spread axially. This occurs at a somewhat higher pressure. Soon, steady-state propagation is reached as seen in configurations ③ and ④. Again, these features of the response were also observed in the experiments (e.g. see Fig. 3[1]).

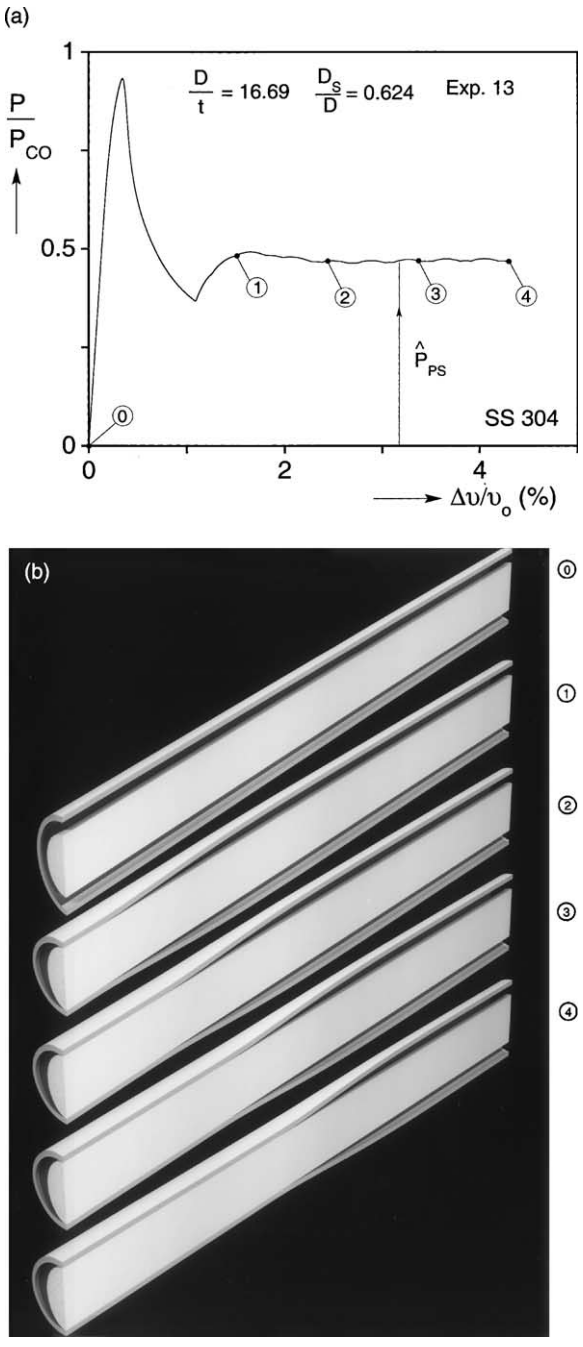

Fig. 18. (a) Calculated pressure-change in volume response for pipe with solid insert simulating Exp. 13. (b) Sequence of collapse configurations corresponding to (a).

The calculated propagation pressure of the two-pipe system ($\hat{P}_{P2}$) is 790 psi (54.5 bar) which is 1.5% higher than the measured value. By contrast, the 2D model yielded a value 8.4% lower than the experiment and Eq. (3) yields a pressure which is 58% of the experimental one.

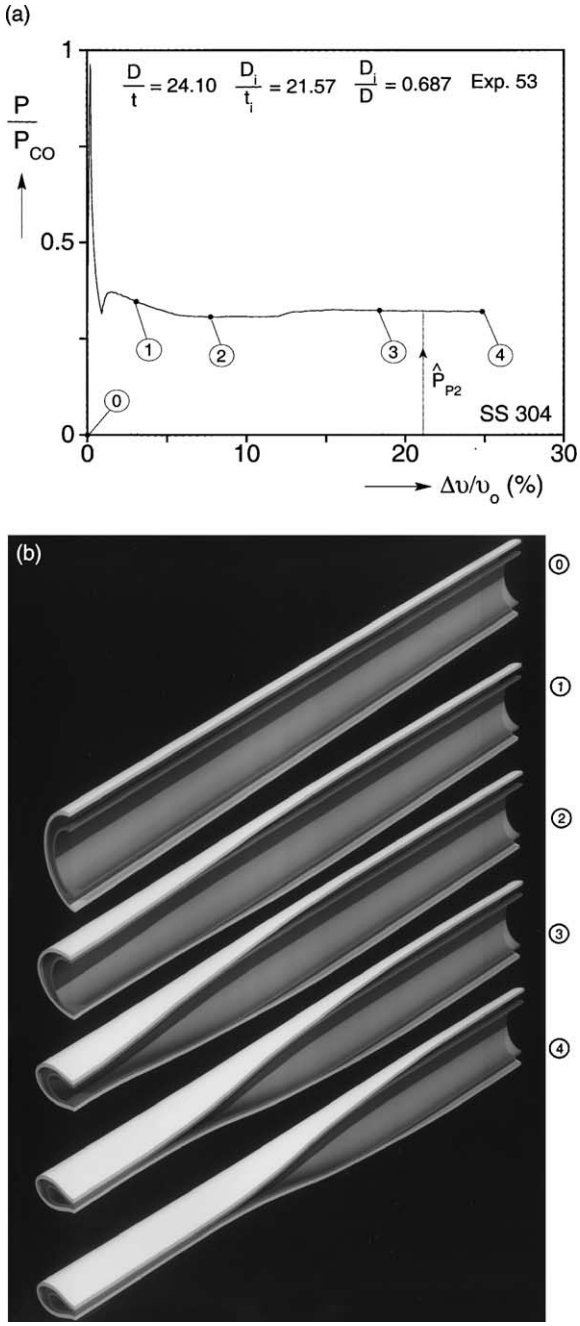

Fig. 19. (a) Calculated pressure-change in volume response for pipe-in-pipe system simulating Exp. 53. (b) Sequence of collapse configurations corresponding to (a).

Three more simulations were performed for pipe-in-pipe systems. They were for Exp. 51 involving a carrier tube with $D/t = 24.0$ and Exps. 23 and 52 for carrier tubes with $D/t = 16.6$. The other parameters of

these cases are listed in Table 3. The predicted values of $\hat{P}_{P2}$ are within 1% of the measured value for Exp. 51 and within 0.8% for Exp. 23. In the case of Exp. 52 the prediction was 5.9% higher than the measured value which we attribute to some small, unknown discrepancy in the stress–strain responses adopted for the two tubes. The quality of the 2D predictions are comparable to those of the other cases and once more those from Eq. (3) are of qualitative value.

3.4. Pipe-in-pipe systems with two quasi-static propagation events

The last simulation we present involves a two-pipe system which in the experiment exhibited two propagation events. The outer tube had a $D/t = 21.78$, the inner one $D_i/t_i = 13.33$ and its diameter was $0.625D$. The thickness of the inner tube was higher than the critical value and thus collapse propagated over the inner tube first leaving it intact. The second propagation of collapse occurred at a higher pressure and involved partial collapse of the inner tube (similar to events described in Fig. 8 [1]). The remaining parameters of the tubes involved are listed in Table 3 along with the two-propagation pressures measured (Exp. 74).

The simulation was carried out very much as described in the previous section. The calculated $P - \Delta v$ response is shown in Fig. 20a and the initial (⓪) and four deformed configurations are shown in Fig. 20b. The initial part of the response is similar to the ones shown earlier. The outer tube collapses in the neighborhood of the imperfection. On first contact with the inner tube, the radial growth of collapse is arrested and spreading along the length starts. The deeper first pressure valley seen in experiments and simulations involving solid inserts is repeated here. A pressure plateau develops at a level of 1096 psi (75.5 bar) indicating steady-state propagation of collapse (depicted in Fig. 20a by $\hat{P}_{P2}\big|_1$). This first spreading of collapse is clearly seen in configurations ① and ②. The collapse reaches the far end of the tubes which are radially clamped and gets arrested. Subsequently the pressure increases and at a level of 1293 psi (89.2 bar) a second initiation event takes place which starts to partially collapse the inner tube. A new steady-state is reached at a pressure of 1255 psi (86.6 bar—indicated in Fig. 20a by $\hat{P}_{P2}\big|_2$). The extent of the deformation of the inner tube can be seen in configurations ③ and ④. It is very similar to what was seen in the experiment. The simulation was terminated before the end of the tubes was reached. The first propagation pressure was 1.7% less and the second 2.9% higher than the measured values.

Overall, the results demonstrate that the propagation pressures of single pipes, pipes with solid inserts and pipe-in-pipe systems can be predicted to a great degree of accuracy using the 3D models developed. The major requirement for this high degree of success is that the geometric and material parameters of the pipes are represented accurately in the models. A small drawback of these models is that they are relatively computationally intensive and, as a result, are not as yet suited for extensive parametric studies of these critical pressures.

4. Summary and conclusions

A new phenomenon of propagation of collapse in pipe-in-pipe systems under external pressure has been studied through combined experimental and analytical efforts. The phenomenon is similar to that known to affect single pipes. Collapse of the carrier pipe is local in nature and can be caused either by excessive loading (pure external pressure or combined with bending and tension loads) or due to local weakening of the pipe by compromising its geometric integrity. This study has demonstrated that for pipes with commonly used geometric and material parameters local collapse of the carrier pipe will usually result in collapse of both pipes. If the external pressure is high enough, the collapse tends to propagate dynamically flattening catastrophically large sections of such lines. In practice, the extent of the damage can be limited by the periodic installation of buckle arrestors along the length of the line.

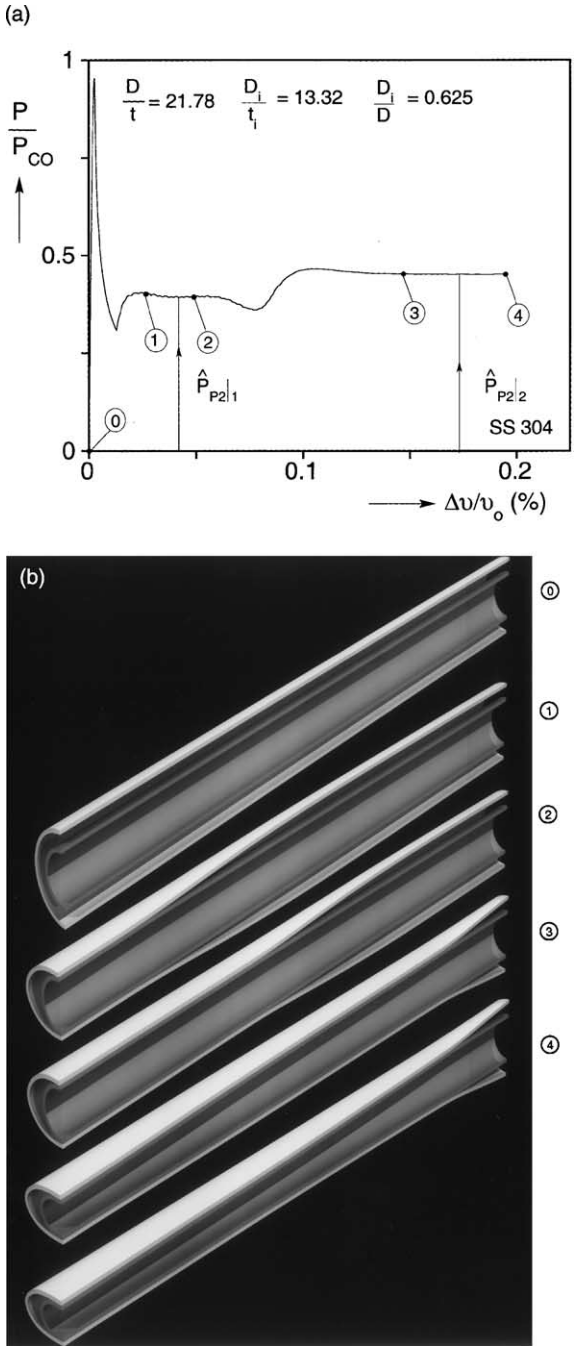

Fig. 20. (a) Calculated pressure-change in volume response for pipe-in-pipe system simulating case with two steady-state propagation events. (b) Sequence of collapse configurations corresponding to (a).

The lowest pressure at which collapse which has been initiated in a pipe-in-pipe system will propagate is the propagation pressure of the system designated in this study by P_{P2}. This is the pressure above which the

line must be protected by buckle arrestors. The dependence of this critical pressure on the geometric and material parameters of the two pipes was studied extensively experimentally and the following empirical relationship was developed for it:

$$\frac{P_{P2}}{P_P} = 1 + 1.095\left(\frac{\sigma_{oi}}{\sigma_o}\right)^{0.4}\left(\frac{D_i}{D}\right)\left(\frac{t_i}{t}\right)^2. \tag{6}$$

This expression represents collapse propagation which affects both pipes. For higher values of inner pipe D_i/t_i the collapse of both pipes is complete whereas for lower values the inner pipe is only partially collapsed (but sufficiently to render it useless).

An interesting second mode of collapse propagation was also discovered in which the carrier pipe collapses leaving the inner one intact. For example, given a carrier pipe and the diameter ratio of the two pipes (D_i/D), P_{P2} increases proportionately to $(t_i)^2$. At some critical value of t_i, propagation of collapse in just the carrier pipe becomes preferable. Propagation of collapse affecting both pipes is still possible but at a higher (usually) pressure level. The pressure at which this switch takes place has been found to closely correspond to P_{PS}, the propagation pressure of a carrier pipe with a solid rod insert of the same diameter as the inner pipe. The following empirical relationship was established for P_{PS}:

$$\frac{P_{PS}}{P_P} = 1 + B\left(\frac{D_S}{D}\right)^{\gamma} \tag{7}$$

($B = 2.116$ and $\gamma = 2.677$).

An important practical use of P_{P2} is in establishing the level of pressure beyond which the system must be protected with buckle arrestors. Although in some cases the collapse may affect only the carrier pipe, prudent design should protect the line against such an eventuality also. Thus, we envision using the empirical relationships (6) and (7) together. Use Eq. (6) to establish P_{P2} for a given pipe-in-pipe system. Use the result to design the pipeline provided $P_{P2} < P_{PS}$. If $P_{PS} < P_{P2}$ then the propagation pressure that should be adopted in the design of the system should be equal to P_{PS}.

Three levels of models were used to estimate P_{PS} and P_{P2}. The simplest models involve kinematically admissible uniform collapse mechanisms resulting from the formation of plastic hinges. These models yield closed-form expressions for these critical pressures which provide a qualitative first impression on how they depend on the main parameters of the problem. The models were, however, found to yield propagation pressures which are significantly lower than measured values and thus they are not recommended for direct use in design.

The second type of model studied also involves uniform (plane strain) collapse of the systems which was conducted numerically. The calculated 2D pressure–volume responses were subsequently used to conduct an energy balance between prebuckling and collapsed configurations. This yields approximate estimates of P_{P2} and P_{PS}. For the pipe parameters used in this study, the predicted propagation pressures are generally lower than measured values although the predictions approach the experimental results for thicker inner tubes. Overall, the predictions are within acceptable engineering accuracy. In view of their relative numerical efficiency, such models can be used to study the parametric dependence of P_{P2} and P_{PS}. The 2D models also reproduced qualitatively the multiple collapse propagation phenomena discovered in the experiments. The transitional value of t_i/t at which they start to occur was underestimated.

The third type model considered involves a detailed, 3D, numerical simulation of the initiation and steady-state propagation of collapse in such systems. It was demonstrated that, provided the geometric and material characteristics of the pipes tested are accurately represented in the models, both P_{P2} and P_{PS} can be predicted to great accuracy. This high degree of accuracy has also been demonstrated in the past to be achievable in similar calculations involving the propagation pressure of single pipes. Because such 3D

calculations are numerically intensive, we envision them being used sparingly, perhaps as a final check of a particular pipe-in-pipe design.

Acknowledgements

The financial support of a group of industrial sponsors through the Joint Industry Project Structural Integrity of Offshore Pipelines is acknowledged with thanks. The numerical calculations were conducted using ABAQUS under academic license from Hibbitt, Karlsson and Sorensen.

References

Chater, E., Hutchinson, J.W., 1984. On the propagation of bulges and buckles. ASME J. Appl. Mech. 51, 269–277.

Dyau, J.Y., Kyriakides, S., 1993b. On the propagation pressure of long cylindrical shells under external pressure. Int. J. Mech. Sci. 35, 675–713.

Hill, R., 1948. A theory of the yielding and plastic flow of anisotropic metals. Proc. R. Soc. A 193, 281–297.

Jensen, H.M., 1988. Collapse of hydrostatically loaded cylindrical shells. Int. J. Solids Struct. 24, 51–64.

Kamalarasa, S., Calladine, C.R., 1988. Buckle propagation in submarine pipelines. Int. J. Mech. Sci. 30, 217–228.

Kyriakides, S., 1993. Propagating instabilities in structures. In: Hutchinson, J.W., Wu, T.Y. (Eds.), Advances in Applied Mechanics, vol. 30, Academic Press, Boston, pp. 67–189.

Kyriakides, S., Arikan, E., 1983. Postbuckling behavior of inelastic inextensional rings under external pressure. ASME J. Appl. Mech. 50, 537–543.

Kyriakides, S., Babcock, C.D., 1981. Large deflection collapse analysis of an inelastic inextensional ring under external pressure. Int. J. Solids Struct. 17, 981–993.

Kyriakides, S., Babcock, C.D., 1981. Experimental determination of the propagation pressure of circular pipes. ASME J. Energy Resour. Technol. 104, 328–336.

Kyriakides, S., Babcock, C.D., Elyada, D., 1984b. Initiation of propagating buckles from local pipeline damages. ASME J. Energy Resour. Technol. 106, 79–87.

Kyriakides, S., Chang, Y.C., 1992. On the effect of axial tension on the propagation pressure of long cylindrical shells. Int. J. Mech. Sci. 34, 3–15.

Kyriakides, S., Yeh, M.K., Roach, D., 1984a. On the determination of the propagation pressure of long circular tubes. ASME J. Pressure Vessel Technol. 106, 150–159.

Netto, T.A., Kyriakides, S., 2000. Dynamic performance of integral buckle arrestors for offshore pipelines. Part II. Analysis. Int. J. Mech. Sci. 42, 1425–1452.

Nogueira, A.C., Tassoulas, J.L., 1994. Buckle propagation: steady-state finite element analysis. ASCE J. Engng. Mech. 120, 1931–1944.

Palmer, A.C., Martin, J.H., 1975. Buckle propagation in submarine pipelines. Nature 254, 46–48.

Park, T.-D., Kyriakides, S., 1997. On the design of integral buckle arrestors for offshore pipelines. Int. J. Mech. Sci. 39, 643–669.

Wierzbicki, T., Bhat, S.U., 1986. On the initiation and propagation of buckles in pipelines. Int. J. Solids Struct. 22, 985–1005.